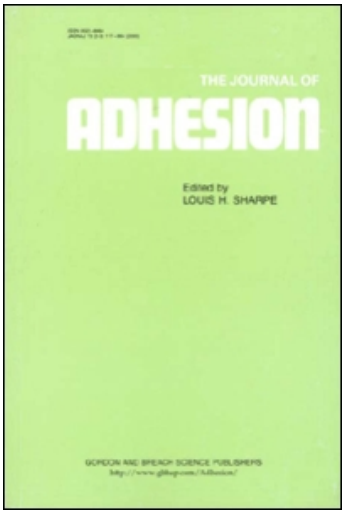

The Journal of Adhesion
Publication details, including instructions for authors and subscription information:
http://www.informaworld.com/smpp/title~content=t713453635

GRADIENT OF THE MECHANICAL MODULUS IN GLASS-EPOXY-METAL JOINTS AS MEASURED BY BRILLOUIN MICROSCOPY

J. K. Krüger[a]; W. Possart[a]; R. Bactavachalou[a]; U. Müller[a]; T. Britz[a]; R. Sanctuary[b]; P. Alnot[c]
[a] Universität des Saarlandes, Saarbrücken, Germany [b] Centre Universitaire de Luxembourg, Luxembourg [c] Laboratoire de Physique des Milieux Ionisés et Applications (LPMIA), Vandoeuvre les Nancy, France

Online publication date: 10 August 2010

To cite this Article Krüger, J. K. , Possart, W. , Bactavachalou, R. , Müller, U. , Britz, T. , Sanctuary, R. and Alnot, P.(2004) 'GRADIENT OF THE MECHANICAL MODULUS IN GLASS-EPOXY-METAL JOINTS AS MEASURED BY BRILLOUIN MICROSCOPY', The Journal of Adhesion, 80: 7, 585 — 599
To link to this Article: DOI: 10.1080/00218460490476973
URL: http://dx.doi.org/10.1080/00218460490476973

The Journal of Adhesion, 80: 585–599, 2004

ISSN: 0021-8464 print/1545-5823 online
DOI: 10.1080/00218460490476973

Taylor & Francis
Taylor & Francis Group

GRADIENT OF THE MECHANICAL MODULUS IN GLASS–EPOXY–METAL JOINTS AS MEASURED BY BRILLOUIN MICROSCOPY

J. K. Krüger
W. Possart
R. Bactavachalou
U. Müller
T. Britz
Universität des Saarlandes, Saarbrücken, Germany

R. Sanctuary
Centre Universitaire de Luxembourg, Luxembourg

P. Alnot
Laboratoire de Physique des Milieux Ionisés et Applications (LPMIA), Université de Nancy I, Vandoeuvre les Nancy, France

The newly developed Brillouin microscopy is used for the first time to measure in situ *the longitudinal elastic stiffness coefficient in the GHz-range inside of glass–epoxy–metal joints as a function of distance from the substrates. Interphases with a local variation of mechanical properties are quantitatively characterized. These interphases possess unexpected widths of tens to hundreds of microns. Inside the interphases, the spatial variation of the longitudinal stiffness coefficient depends on the type of substrate, on the curing conditions for the epoxy and probably on the distribution of internal stresses. The obtained spatial mechanical profiles provide valuable insight into the morphology-driven mechanics of the interphase, but additional information is needed for a full understanding of their physical and chemical origin. The presented results prove the sensitivity of the Brillouin microscopy; the elastic stiffness coefficients are detected with an accuracy in the subpercentage range. The spatial resolution is better than 10* μ*m.*

Keywords: Epoxy; Brillouin microscopy; Mechanical modulus; Epoxy-metal interphase

Received 11 August 2003; in final form 19 March 2004.

This work was kindly supported by the Deutsche Forschungsgemeinschaft. R. Sanctuary is indebted to the Ministère de la Culture, de l'Enseignement Supérieur et de la Recherche du Grand-Duché de Luxembourg for additional funding.

Address correspondence to Wulff Possart, Universität des Saarlandes, Gebaude 22, 6 Etage, Postfach 151150, D-66041, Saarbrücken, Germany. E-mail: w.possart@rz.uni-sb.de

INTRODUCTION

It is generally accepted that polymer adhesives form interphases at the contact with their adherends [1–10]. These interphases play a key role for the technical performance of an adhesive joint since they possess peculiar physical and chemical properties that can deviate considerably from the bulk. This is especially true for reactive adhesives since they form their polymer structure under the influence of the substrate. However, experimental access to these interphases is still a most difficult task. Usually, people try to get information on interphases by investigating adhesive films of varying thickness or by studying fracture surfaces or cross sections of adhesive joints.

So far, the *mechanical* response can be investigated only for an adhesive joint as a whole. In addition, customary experimental techniques are not sensitive enough for the study of very thin films. The contactless and nondestructive experimental access to the elastic properties of these interphases is a most difficult task. Adhesives are designed to provide strong adhesive coupling with the substrate surface on the molecular level. As a consequence, the interphase will possess a characteristic morphology, and the mechanical properties are expected to be different from those of the inner part of the adhesive layer, not to mention the bulk state of the adhesive.

Recently, we described a μ-Brillouin spectrometer with a theoretical spatial resolution close to 1 μm [11]. Depending on the laser beam diameter (*ca.* 10 μm) and on properties of the sample such as homogeneity, surface roughness and elasto-optical coupling, the scattering volume in this article is estimated to be about $10 \times 5 \times 5\,\mu m^3$. This new Brillouin microscopy is a nondestructive, noncontact technique for transparent adhesives. We present first measurements for adhesive joints *glass–epoxy–metal* with particular emphasis on the mechanical modulus of the interphases.

EXPERIMENTAL

The samples are prepared as 1 mm thick plates of an epoxy adhesive cured between a glass slide and a 100 nm metal film that is supported by a silicon wafer. The metal film is made by physical vapor deposition of pure Al, Cu, or Au. The Al and the Cu films are covered with their native oxide layers of 2–3 nm thickness and a ubiquitous hydrocarbon layer. The Au surface carries traces of adsorbed water and a similar carbonaceous layer. For the epoxy, 100 parts (by mass) of diglycidylether of bisphenol A (DGEBA) and 14 parts of diethylene triamine (DETA) are stirred intensively at 55°C for 5 min. This mixture is cured

at 23°C between the surfaces of the glass and the metal for 48 h. In the bulk, this curing is incomplete (epoxy group consumption only 73% as measured by IR spectroscopy) and the cured polymer has a pycnometric density of $1.17\,\mathrm{g\,cm^{-3}}$.

The technical details of the Brillouin microscope (BM) are described elsewhere [11]. Briefly, it makes use of a high performance tandem Brillouin spectrometer of the Sandercock type [12]. The apparatus is fully computer controlled, including the temperature stabilization of the Fabry-Pérot interferometer. Long-term measurements of very weak signals are therefore possible. The free spectral range is 30 GHz in all epoxy measurements reported here. The measurable frequency range was adjusted to ± 20 GHz by the scan voltage. For usual scattering intensity, the frequency of the spectral lines is determined with an accuracy of 0.01%.

Basically, Brillouin spectroscopy is a light-scattering method. A laser beam (wave vector $\vec{\mathbf{k}}_\mathrm{i}$, vacuum wave length λ_0, wavelength in the sample $\lambda_\mathrm{i} = \lambda_0/\mathrm{n_{sample}}$, frequency $\omega_\mathrm{i} = 2\pi \mathrm{f_i}$; in this work green light with $\lambda_\mathrm{o} = 532\,\mathrm{nm}$ and $\mathrm{f_i} \approx 5.64 \cdot 10^{14}\,\mathrm{Hz}$) hits the transparent sample, and the spectrum of the scattered light is recorded for defined geometric conditions. For the BM, a sketch of the preferred scattering geometry is given in Figure 1. The adhesive joint must have a smooth surface from where the laser light can transit the adhesive. For our samples, this condition is obeyed by the glass slide that is used as one of the adherends.

The incident laser beam is slightly focused on the metal surface, where it has a diameter of about 10 μm. Through the glass plate (gp) the scattered light (wave vector $\vec{\mathbf{k}}_\mathrm{s}$) is transmitted onto the objective of a customized microscope (maximum magnification 140), which is focused on the laser beam. As the result of this microscope optics, an area with a diameter of $\geq 1\,\mu\mathrm{m}$ can be selected from the laser beam and the scattered light is focused on the entrance pinhole of the Brillouin spectrometer. The strong magnification of the microscope results in a very low focal depth. As a rough estimate, we get a scattering volume (sv) of $\geq (1 \times 1 \times 10)\,\mu\mathrm{m}$. In this work, an image cross section of about 5 μm diameter is used. Hence, we end up with a sv of roughly $5 \times 5 \times 10\,\mu\mathrm{m}^3$. It can be shifted along the incoming laser beam by rotating the glass plate gp (dotted arrow in Figure 1). This provides a positioning accuracy of 0.1 μm. Parallel to the metal surface, the sv can be located at every point by moving an x,y stage (arrow shown in Figure 1). The angle α defines the direction from which scattered light is collected by the entrance optics (in our case: $\alpha = 43^\circ$). α corresponds to a defined light-scattering angle, θ, inside the scattering volume [14, 15],

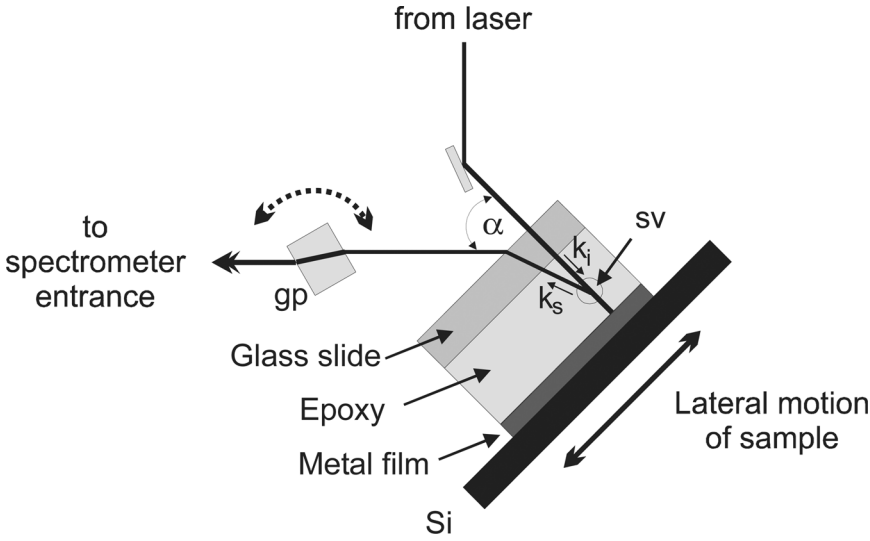

FIGURE 1 Reflection scattering geometry for Brillouin microscopy: $\vec{k}_i$, wave vector of the incoming laser light; $\vec{k}_s$, wave vector of the scattered laser light; $180^\circ - \alpha$, external scattering angle; Si, silicon wafer; sv, scattering volume; gp, glass plate.

$$\theta = \left[\pi - \arcsin\left(\frac{\sin\alpha}{n}\right)\right], \tag{1}$$

where n is the refractive index of the epoxy. In Equation (1), refraction in the glass slide on top of the epoxy is neglected because $n_{glass} \approx n_{ep}$.

Since the lateral dimensions of the sv are large compared with the acoustic wave length, the Brillouin spectrum consists of the elastically scattered Rayleigh line ($\omega = \omega_i$) and of six lines (at maximum) for inelastically scattered photons with frequencies $\omega_p\left[\vec{k}_i, \vec{k}_s(\theta)\right]$ ($\vec{k}_i = \text{const.}$, $\vec{k}_s(\theta) = \text{const.}$, index $p = 1 \ldots 6$)—see Figure 2a for a typical spectrum recorded for the epoxy on Al.

The photons have been scattered at hypersonic waves that are permanently generated by thermally excited density fluctuations in the sample. These sound waves correspond to three acoustic phonons (at maximum) that are defined by their common wave vector, $\vec{q}$, and by their frequencies, Ω_r. According to the conservation laws for energy and momentum, we have

$$\omega_p = \omega_i \pm \Omega_r \qquad r = 1 - 3 \tag{2}$$

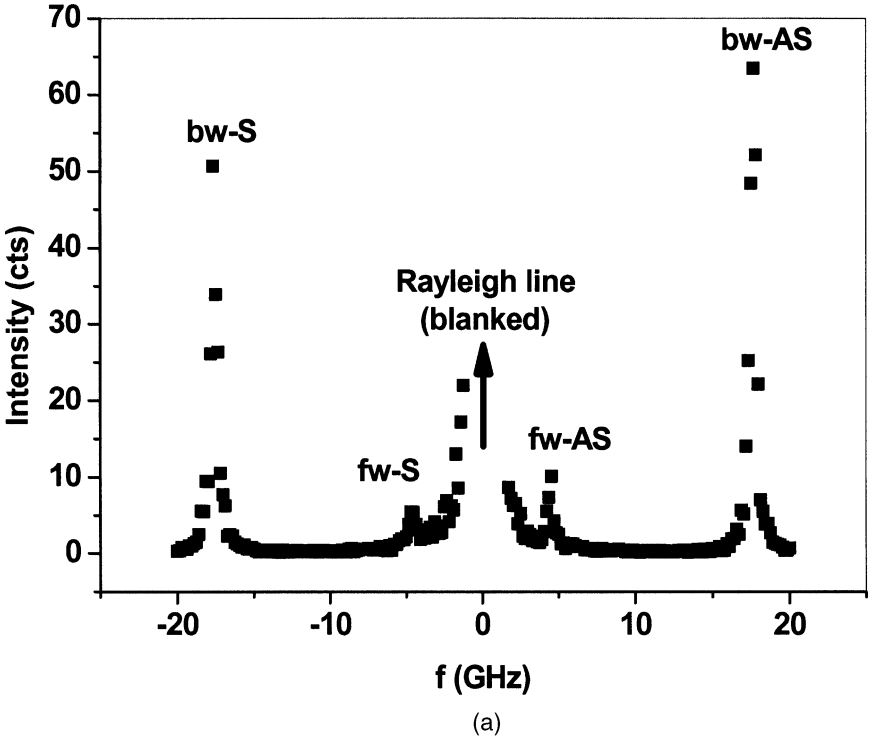

FIGURE 2 A selection of Brillouin spectra measured inside a room temperature cured epoxy layer (1 mm thick) as a function of position. (a) Full Brillouin spectrum (frequency scale $f = f_{laser} - f_{scattered\ photon}$). The Rayleigh line (at $f = 0$) is blanked. The inelastic lines are marked for the Stokes (S) and for the Antistokes (AS) region. The lines "bw-S" and "bw-AS" correspond to photons scattered from the incident ($+\vec{k}_i$) and from the reflected ($-\vec{k}_i$) laser light, respectively (see Figure 1 and Eq. (2) for the scattering geometry). (b) Spectral lines "bw-AS" at four different positions d (in μm, $d = 0$ at the interface glass−epoxy) of sv inside the epoxy layer. As an example, 2Γ marks an optical line width at half maximum (before deconvolution). (Continued.)

for the scattered light with the Ω_r in the range of some GHz, and

$$\vec{q} = \vec{k}_i \pm \vec{k}_s \quad \text{with} \quad q = \frac{4\pi n}{\lambda_i} \tag{3}$$

with a typical acoustic wave length $\lambda_{acoust} = \dfrac{2\pi}{q}$ of some 100 nm. As the result, the ω_p values are very close to ω_i.

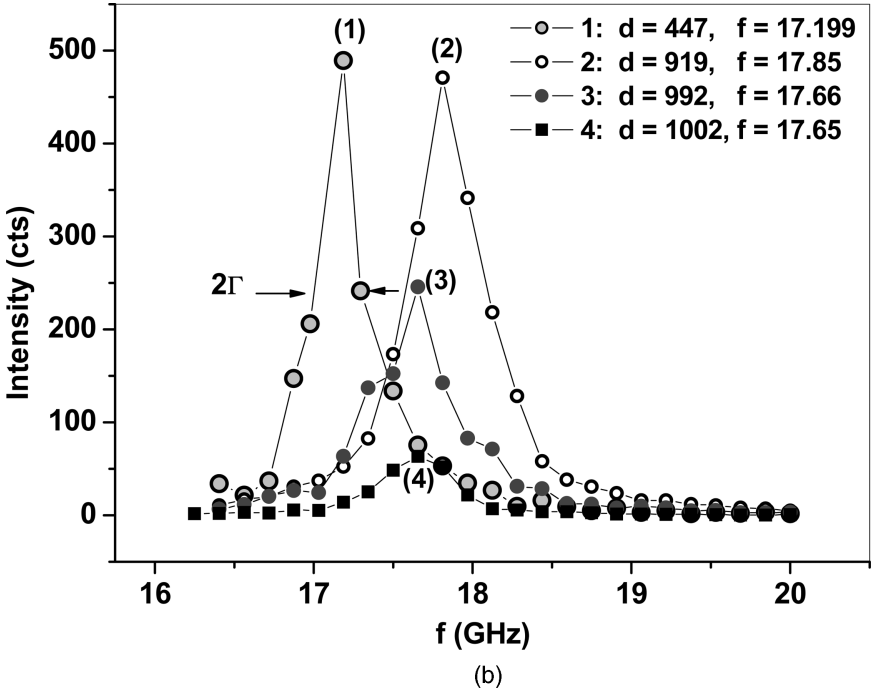

FIGURE 2 (Continued).

Each spectral line at ω_p possesses a full width at half maximum (FWM) $2\Gamma_p$. From Γ_p, the attenuation Γ_r of the propagating sound wave is obtained by deconvolution with the transmission function of the spectrometer (Gaussian line with FWHM ≈ 0.2 GHz for the given experimental conditions). We note in passing that polymers show noticeable hypersonic damping even in the glassy state [12, 13].

The hypersonic velocity of each sound wave is given by

$$\vec{v}_r = \frac{\Omega_r}{q} \cdot \vec{e}_r. \tag{4}$$

For an isotropic sample, only two phonon frequencies are observed. With the mass density ρ for the material in the isotropic scattering volume, the elastic stiffness coefficients c_{11} for longitudinal deformation and c_{44} for shear deformation are calculated from

$$c_{11} = \rho \cdot v_1^2, \qquad c_{44} = \rho \cdot v_2^2, \tag{5}$$

with v_1, v_2 as the sound velocities of the longitudinal and the transverse sound modes, respectively.

In the bulk, the stiffness coefficients are related to the elastic moduli E (Young), G (shear), and K (compression), and to the Poisson ratio, ν, by

$$E = c_{44}\left(4 + \frac{c_{11}}{c_{44} - c_{11}}\right), \qquad G = c_{44}, \qquad K = c_{11} - \frac{4}{3c_{44}},$$
$$\nu = \frac{c_{11} - 2c_{44}}{2(c_{11} - c_{44})}. \tag{6}$$

These parameters describe the mechanical behavior of the adhesive at hypersonic frequencies inside the scattering volume.

For the BM with the scattering geometry given in Figure 1, the longitudinal sound velocity, v_1, of the isotropic sample can be calculated from the measuring angle, α, by

$$v_1 = \frac{\Omega_1}{q} = \frac{f_1 \cdot \lambda_0}{2 \cdot n \cdot \sin\left\{\frac{1}{2} \cdot \left[\pi - \arcsin\left(\frac{\sin\alpha}{n}\right)\right]\right\}}, \tag{7}$$

where f_1 is the sound frequency of the longitudinal sound mode [12, 14, 15]. Since the spatial dependence of the refractive index, n, of the epoxy is not known, we take the average bulk value ($n = 1.594$) for the calculation of v_1. This is a good approximation for the following reason. Room temperature curing causes just a 1.8% increase of n for the transition from the liquid to the glassy state. The major part of this change in n (*ca.* 1.6%) occurs in the early stages of curing while the system is visco-elastic. Postcuring adds only another 0.1% to n. Inspection of the epoxy layers with a polarized light microscope does not indicate any optical inhomogeneity. Hence, as a conservative estimation for glassy epoxy samples, any variation of f_1 larger than about 0.3% has to be attributed to changes in v_1, which are due to changes in the elastic properties. Because only longitudinal phonon modes are discussed in this article, the subscript of v is omitted.

RESULTS AND DISCUSSION

For the glass–epoxy–Al system as an example, Figure 2b provides some Brillouin spectra of the epoxy at various distances, d, from the glass–epoxy interface. The line intensity is constant for large distances between the sv and the metal, *c.f.* lines Nos. 1 and 2. The intensity of lines Nos. 3 and 4 goes down, while the frequency stays almost constant because the metal interface starts to reduce the sv for these positions.

Figure 3 shows that the corresponding sound velocity data v, Γ are well resolved within the epoxy by Brillouin microscopy. The sound attenuation is constant throughout the epoxy, but the sound velocity forms a d-profile.

First of all, it has to be proven that this profile is not a kind of artefact. Figure 4 provides the corresponding data for v and Γ inside liquid DGEBA ($\rho = 1.157\,\mathrm{g\,cm^{-3}}$) within a distance of 250 μm from the Al substrate.

Neither the velocity nor the attenuation of the longitudinal sound mode depend on the measuring position in the liquid. There is only some scatter due to the small light-scattering cross section of DGEBA. This is exactly the result that is to be expected for an isotropic liquid. Any interaction with a solid interface will not exert a long-range effect on the structure or on the density of the liquid but it will be confined to the molecular level. Hence, this simple experiment proves that there are no pitfalls in our Brillouin microscopy.

Therefore, we conclude that the d-profiles given in Figure 3 depict real spatial dependencies of sound velocity and sound attenuation in

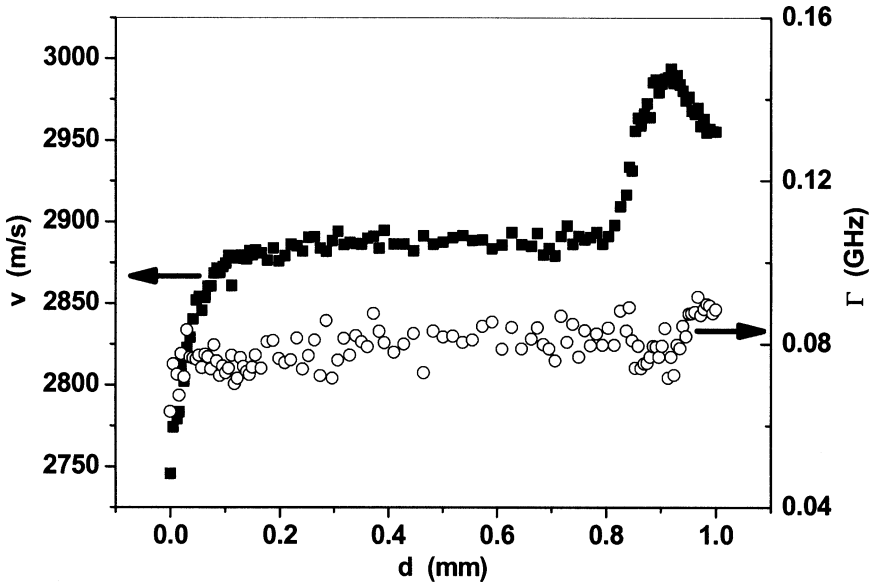

FIGURE 3 Longitudinal sound velocity, v (black squares), and attenuation, Γ (open circles), in an epoxy plate cured between a glass slide (interface at d = 0 mm) and a silicon wafer covered with Al (interface at d = 1 mm) as a function of the position, d, of the scattering volume normal to the glass–epoxy interface.

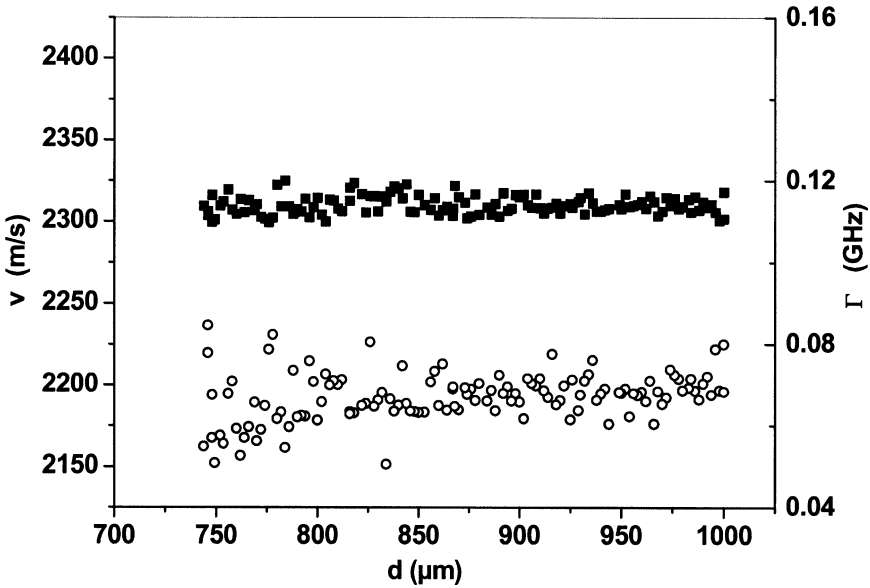

FIGURE 4 Longitudinal sound velocity, v (black squares), and attenuation, Γ (open circles), inside a 1 mm layer of liquid monomer DGEBA on an Al surface (at d = 1000 μm).

the epoxy network. $\Gamma(d) \approx$ const reveals that the changes in v(d) are not caused by hypersonic dynamics in the epoxy. The v-profile clearly demonstrates that the oxidized Al and the glass exert a different influence on the mechanical properties inside the cured epoxy layer. At the glass interface, the sound velocity is reduced by *ca.* 5% as compared with the average plateau value of $\langle v \rangle = 2888\,m \cdot s^{-1}$, whereas the Al_2O_3 interface induces an increase of about 2.3 %. At some 85 μm distance from the aluminium, the sound velocity goes through a maximum that exceeds the plateau value by 3.7%. All these v-changes are larger than the estimated 0.3% that could be caused by variations of the refractive index (*c.f.* the discussion on Equation (7)). It is really surprising that the mechanical properties of the epoxy at the glass and at the aluminium side possess spatial dependence across regions as broad as *ca.* 155 μm and 220 μm, respectively. These regions are the interphases in terms of mechanical behavior. To the best of our knowledge, such a profile has not been measured *in situ* before. Due to the much smaller range of any molecular interaction, it is obvious that these "mechanical" interphases are not directly related to any kind of fundamental adhesion. The v-minimum at the glass–epoxy interface

could result from plasticization of the network due to some unknown interaction between the glass and the DETA.

Figures 5 and 6 provide the results for the corresponding measurements of the mechanical profile in the glass–epoxy–copper and in glass–epoxy–gold samples as compared with the glass–epoxy–aluminium joint. For these graphs, Equation (5) is applied with the bulk density, $\rho_{ep} = 1.17\,g\,cm^{-3}$, for an estimation of the high-frequency elastic stiffness coefficient, c_{11}. This estimate makes sense for the following reasons. During room temperature cure, ρ_{ep} increases in total by 3.9%, but the first 3.5% of this shrinkage appears in the liquid state in the early stages of reaction. A postcuring step (120°C for 1 h) that causes full epoxy group consumption would add a negligible rise of density (+0.3%). Hence, the change of ρ_{ep} is estimated to be less than 1% in the solid state.

Inside the epoxy layers (Figure 5), the plateau values $\langle c_{11} \rangle$ differ by less than 1% ($\langle c_{11} \rangle = 9.75$ GPa on Al, $\langle c_{11} \rangle = 9.66$ GPa on Cu). At the metal side, it does not matter much for the c_{11}-profile in the adjacent

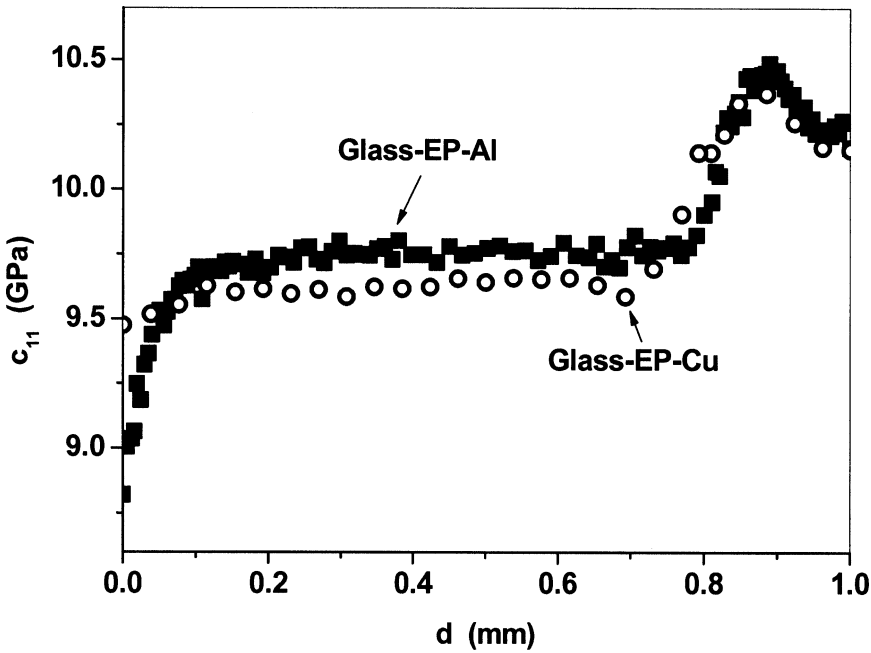

FIGURE 5 Elastic stiffness coefficient, c_{11}, as a function of d inside the epoxy layer cured between Al (black squares) or Cu (open circles) on one side and a glass slide on the other (glass–epoxy interface at d = 0 mm).

interphase whether the epoxy is in contact with the aluminium oxide or with the copper oxide: The maximum in c_{11} is about 107% of the corresponding plateau value and at the metal interfaces we have $c_{11} \approx 1.05 \cdot \langle c_{11} \rangle$. The Cu interphase appears to be somewhat broader (*ca.* 300 μm) than the Al interphase (*ca.* 230 μm). At the glass side of the copper sample, the drop of c_{11} almost disappeared, however. We suppose that appearance and profile of a mechanical interphase are also sensitive to the state of the glass surface, which was not controlled explicitly in these experiments. Further experiments are needed for clarification of this aspect.

Figure 6 provides the c_{11}-profile in the Au–epoxy–glass system. The plateau value $(\langle c_{11} \rangle \approx 9.84\,\text{GPa})$ is almost the same as for the Al sample (less than 1% higher), but c_{11} tends to depend slightly on position in the epoxy on Au. At the glass side, the interphase is present again with about the same drop of c_{11} as for the Al–epoxy–glass sample but with a much reduced width (*ca.* 25 μm). At the Au side, the interphase extends only to some 190 μm into the epoxy, and the stiffness value at the maximum (located at $d \approx 930\,\mu\text{m}$) is closer to the interface than on the Al oxide (at *ca.* 880 μm).

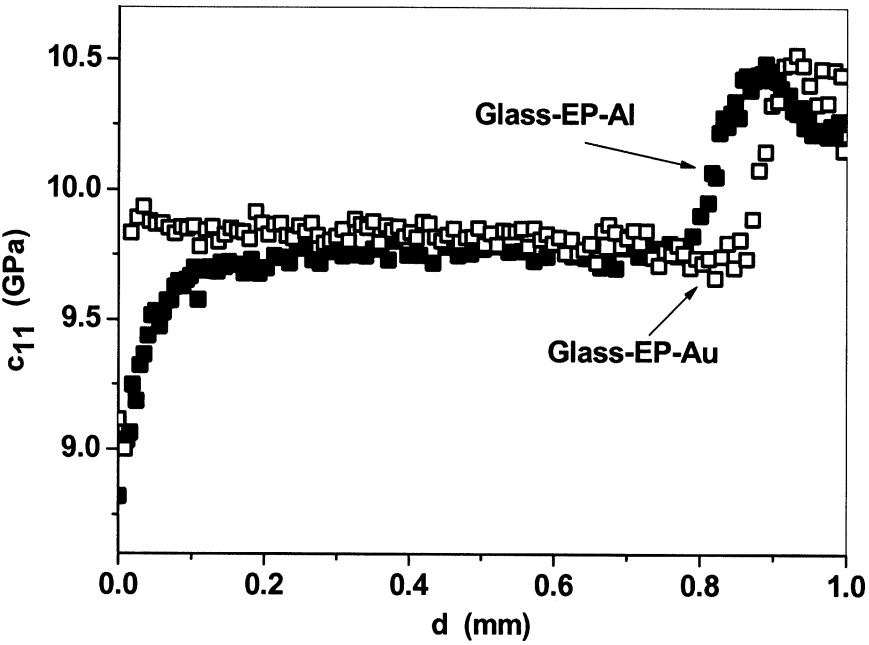

FIGURE 6 Elastic stiffness coefficient, $c_{11}(d)$, inside the epoxy between Al (black squares) or Au (open squares) as for Figure 5.

It is not easy to understand what makes the mechanical interphases so broad, *i.e.*, what causes such a long-range influence from the substrate interfaces into the epoxy during the curing process.

We start discussion with a consideration of structural influences. All specimens show reasonable mechanical strength. According to some articles in the literature [16–22] and to our own results, several amines tend to enrich at aluminium interfaces. This could lead to a more dense epoxy network, but the following observations are in conflict with this simple expectation. Amine groups undergo some kind of chemisorption or may even form organo-metal complexes with Al and Cu that diffuse into the adhesive. Consequently, the curing chemistry is disturbed, and this produces an incomplete network. For ultrathin epoxy films ($d < 200\,nm$) a reduced glass transition temperature is found [8]. Up to now, the length scale of these effects is not precisely known, but our preliminary results point to a range in the order of $10^2\,nm$ rather than $10^2\,\mu m$. Obviously, it is not straightforward to correlate the observed mechanical behavior with cited results on the network structure. The narrower interphase on gold indicates that the structuring process was more hindered to propagate into the epoxy than for the other metals.

The reduced c_{11}-coefficient in the polymer–glass interphase (see Figures 5 and 6) suggests a less stiff epoxy network, as could be formed when the curing agent depletes. Here, additional investigations are needed to reveal the source of this effect.

The stiffness maximum at all three metals is even more difficult to explain. Obviously, at least two competing processes have been at work during the formation of the polymer network, but they are not yet identified. One can think of a metal-induced orientation and packing of polymer segments that affects the magnitude of the modulus. In that context, it is important to note that we get an *effective* stiffness coefficient from the Brillouin data. Internal stresses should appear at the metal–epoxy interface due to shrinkage during the polymerisation process. They will also affect the stiffness coefficient as is elucidated by the results shown in Figure 7.

The upper graph depicts $c_{11}(d)$ in an epoxy layer that was cured and postcured in argon atmosphere on a Teflon® substrate. Postcuring caused a larger $\langle c_{11} \rangle$ ($\approx$10.4 GPa). Teflon provides a hostile substrate for the epoxy system because it is not wetted by the monomers and because the network does not adhere to it. Hence, this substrate does not force any adsorption or demixing, and internal stresses are reduced to a minimum because the epoxy can shrink without hindrance. Indeed, $c_{11}(d)$ is almost constant at the Teflon side with no hint of an interphase. At the phase boundary to argon, a steady rise

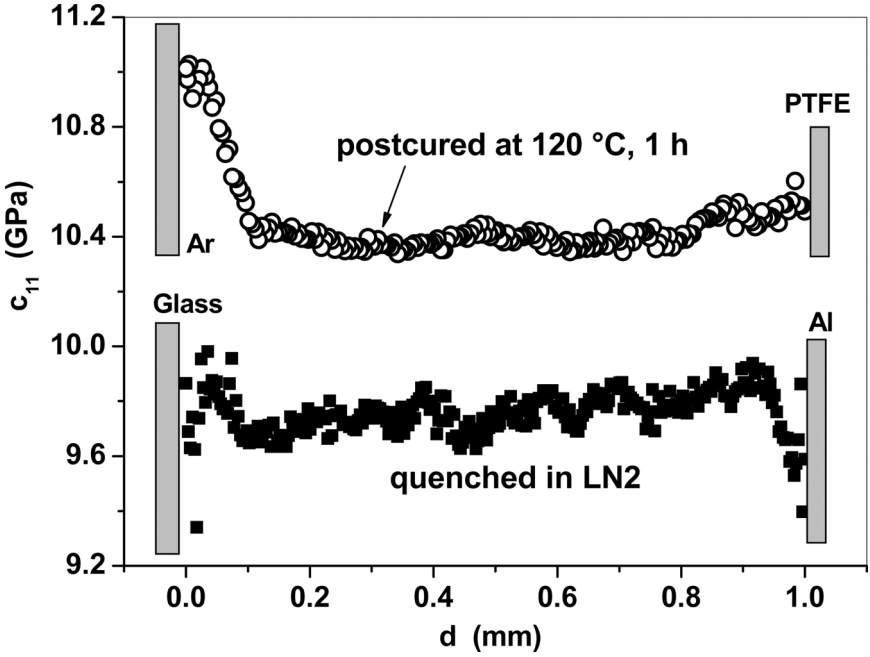

FIGURE 7 *Upper graph:* $c_{11}(d)$ inside the epoxy after curing at 23°C and additional postcuring (120°C for 1 h) on Teflon® with argon as the contacting atmosphere at the top surface. *Lower graph:* $c_{11}(d)$ in the system glass–epoxy–Al after curing at 23°C and quenching in liquid nitrogen where the Al layer delaminated from the Si wafer.

is found for the modulus. It is supposed that this increase of c_{11} could result from a migration of DETA due to partial immiscibility of the amine with DGEBA or with the oligomers that emerge in the early stages of polyaddition. Increased concentration of amines should give an interphase with higher crosslinking density and, hence, improved stiffness. The lower graph of Figure 7 shows $c_{11}(d)$ in a room-temperature–cured Al–epoxy–glass sample after quenching in liquid nitrogen. The glass plate still sticks well on the epoxy, while the shock-freezing caused separation mainly at the wafer–Al interface and at some places the thin Al film was also removed from the epoxy. As compared with the intact joint, the plateau value $\langle c_{11} \rangle$ has not changed significantly for the quenched sample. Only the scatter increased. However, the c_{11}-maximum dropped to *ca.* $1.02 \cdot \langle c_{11} \rangle$ and can hardly be discriminated from the scattering of $c_{11}(d)$. At the Al substrate, c_{11} goes down to about 9.4 GPa, which is a much lower value

than before removal from the Si wafer. Certainly, the internal stresses relaxed to a great extent, and this could explain the changes in c_{11}. Further studies are necessary on the role of the quenching process.

CONCLUSION

The newly developed Brillouin microscopy makes it possible to characterize *in situ* the profile of the mechanical modulus in substrate–adhesive–substrate systems provided the adhesive and one of the substrates possess sufficient transparency. It turns out that different substrates create mechanical interphases of unexpected width and quite different behavior. The obtained spatial profiles of the longitudinal sound velocity give valuable insight into the morphology-driven mechanics of the interphase, but additional information is needed for a full understanding of their physical and chemical origin. The presented results are preliminary since we have neither investigated the transverse sound velocities nor the angle dependence of the sound modes at fixed space coordinates. These additional experimental capabilities will strongly improve the power of Brillouin microscopy. Moreover, it will be of great interest to study the glass transition behavior within the interphases.

REFERENCES

[1] Sharpe, L. H., *J. Adhesion* **4,** 51 (1972).
[2] Bischof, C. and Possart, W., *Adhäsion—Theoretische und Experimentelle Grundlagen*, (Akademie-Verlag, Berlin, 1983).
[3] Lotfipour, M., Reeves, L. A., Kiroski, D., and Packham, D. E., *J. Adhesion* **47**, 33–40 (1994).
[4] Kraus, R., Wilke, W., Zhuk, A., Luzinov, I., Minko, S., and Voronov, V., *J. Mater. Sci.* **32**, 4397–4403 (1997).
[5] Possart, W. and Schlett, V., *J. Adhesion* **48**, 25–46 (1995).
[6] Possart, W., Dieckhoff, S., Fanter, D., Gesang, T., Hartwig, A., Höper, R., Schlett, V., and Hennemann, O.-D., *J. Adhesion* **57**, 227–244 (1996).
[7] Mäder, E., Mai, K., and Pisanova, E., *Composite Interfaces* **7**, 133–147 (2000).
[8] Possart, W. and Krüger, J. K., Adhesion, network formation and properties of curing adhesives in the interphase to metals, In: *Proc. 25th Ann. Meet. Adh. Soc., WCARP II*, Pocius, A. V. and Dillard, J. G., Eds. (The Adhesion Society, Blacksburg, VA 2002) pp. 104–106.
[9] Possart, W. and Krüger, J. K., In: *Proc., EURADH* 2002: 6th *European Adhesion Conference and ADHESION* '02: 8th *Int. Conf. on the Science & Technology of Adhesion and Adhesives*, (The Institute of Materials, IOM Communications, London, 2002) 10–13 September, pp. 7–8.
[10] Bouchet, J., Roche, A. A., Jacquelin, E., and Scherer, G. W., In: *Adhesion Aspects of Thin Films*, Mittal, K. L. Ed. (Brill Academic Publishers, Leiden, Netherlands, 2001). Vol. 1.

[11] Sanctuary, R., Bactavachalou, R., Müller, U., Possart, W., Alnot, P., and Krüger, J. K., *J. Phys. D: Appl. Phys.* **36**, 2738–2742 (2003).
[12] Krüger, J. K., In: *Optical Techniques to Characterize Polymer Systems*, Bässler, H., Ed. (Elsevier, Amsterdam, 1989), pp. 429–534.
[13] Matsukawa, M., Othori, N., Nagai, I., Bohn, K. P., and Krüger, J. K., *Jap. J. Appl. Phys.* **36**, 2976 (1997).
[14] Hayes, W. and Loudon, R., *Scattering of Light By Crystals* (John Wiley, New York, 1978).
[15] Chu, B., *Laser Light Scattering* (Academic Press, New York, 1974).
[16] Dillingham, R. G. and Boerio, F. J., *J. Adhesion* **24**, 315–335 (1987).
[17] Fauquet, C., Dubot, P., Minel, L., Barthes-Labrousse, M.-G., Rei Villar, and Villatte, M., *Appl. Surf. Sci.* **81**, 435–441, (1994).
[18] Barthes-Labrousse, M.-G., *J. Adhesion* **57**, 65–75, (1997).
[19] Bouchet, J., Roche, A. A., and Jaquelin, E., *J. Adhesion Sci. Technol.* **15**, 321–343 (2001).
[20] Bentadjine, S., Petiaud, R., Roche, A. A., and Massardier, V., *Polymer* **15**, 6271–6282 (2001).
[21] Bouchet, J. and Roche, A. A., *J. Adhesion* **78**, 799–830 (2002).
[22] Roche, A. A., Bouchet, J., and Bentadjine, S., *Int. J. Adhesion Adhesives* **22**, 431–441 (2002).